International Journal of Advanced Structural Engineering (2022) 12: 616–630

ORIGINAL RESEARCH

Evaluation of shape factor effect on hysteresis behavior of elastomeric rubber bearings

Ehsan Kazeminezhad*[1], Soroush safakhah[2]

Base isolation is an appropriate approach to mitigate the seismic hazards. A common type of elastomeric rubber bearing is included rubber pads, intermediate steel plates and steel end plates (anchor plates). The hysteresis behavior of elastomeric rubber bearings is affected by vertical pressure and shape factor. In this study cyclic loading is applied and hysteresis behavior in the first and second cycles is evaluated. Finite element method with ABAQUS software is used and validation analysis was done. The results show that second cycle of force-displacement in the elastomeric rubber bearings is more stable than the first cycle and vertical pressure and shape factor influenced damping and hysteresis behavior. Also, elastomeric rubber bearings with lower shape factor have higher damping in comparison with larger shape factor and increase in vertical load led to increase in the damping. The innovation of this paper is adopted various hysteresis parameters in finite element analysis to achieve closest results in comparison with experimental work.

Keywords: Elastomeric rubber bearing; hysteresis behavior; shape factor; vertical pressure; cyclic loading; damping.

Introduction

Earthquakes are unpredictable phenomena that seriously threaten buildings, vital equipment and human lives. Hence, engineers have tried to decrease earthquake damages by new technologies. Base isolation is one of these approaches which can mitigate the seismic forces and prevent transmission to buildings and structures. In general, two different base isolators are existing: elastomeric rubber bearing (EB) and lead rubber bearing (LRB). EBs consist of rubber and steel layers. Steel layers are lie between rubber pads and in the top and bottom of EBs rubber layers are connected to anchor steel end plates. EBs behavior are dependent on several important properties

2

such as vertical stiffness, shear displacement, shape factor and vertical pressure. A lot of study were done on the elastomeric rubber bearings. In the past three decades, numerous studies have been addressed the base isolation technique with particular attention to the elastomeric bearings (EB) with a key role in supporting the structures, especially under the mutual effects of vertical and horizontal loads. Various theories have been also developed to describe the mechanical properties and basic behavior of EBs (elastomeric bearings). The first contribution to the issue of buckling was presented by Haring's theory [1] which was based on the column buckling theory to

✉ Corresponding author: ehsan-kazeminezhad@iauahvaz.ac.ir
1. Department of Civil Engineering, Ahvaz Branch, Islamic Azad University, Ahvaz, Iran.
2. Department of civil engineering, Semnan branch, Islamic Azad University, Semnan, Iran.

account for shear deformation. Kelly [2] developed a theory to find relationships for critical loading and proposed a new isolator calculation. On the other hand, several experimental tests have been conducted ([3]-[13]) demonstrating that vertical and horizontal stiffnesses are related to the increase of lateral displacement. Moreover, numerical simulations have been carried out as an approach to assess the role of nonlinear effect in critical and post-critical mechanisms of EBs ([14]-[19]). Numerical studies have been conducted on EBs using several platforms, such as Abaqus/ CAE and Opensees ([20]-[24]). Recently [25-27] proposed a comparison between numerical findings and the theoretical equation by [28] which illustrated the influence of large deformations on the interaction between horizontal and vertical loads and assessed the post-buckling behavior of EB by extending the original two-spring model of the bearing, developed by [2] and [29]. Applications of EB to buildings were also the subject of research contributions and showed that EBs led to decrease in spectral acceleration by lengthening the main period of buildings [30-35]. In particular, [36] investigated the lateral stability and shear failure limit states of isolated bridge. A 3D numerical simulation was conducted on elastomeric bearings for use in the bridges[37]. Bhuiyan et al. [48] presented a rheology model of high damping rubber bearings for seismic analysis and identify the nonlinear viscosity. In this study cyclic loading is applied and hysteresis behavior in the first and second cycles is evaluated. Finite element method with ABAQUS software is used and validation analysis was done. The results show that second cycle of force-displacement in the elastomeric rubber bearings is more stable than the first cycle and vertical pressure and shape factor influenced damping and hysteresis behavior. Also, elastomeric rubber bearings with lower shape factor have higher damping in comparison with larger shape factor and increase in vertical load led to increase in the damping. The innovation of this paper is adopted various hysteresis parameters in finite element analysis to achieve closest results in comparison with experimental work then based on achieved hysteresis parameters, isolators with various shape factor and vertical pressure subjected to cyclic loading and their damping were evaluated.

1. Numerical modeling

ABAQUS [39] is used in this research to perform numerical simulation adopting three dimensions finite element (FE) approach. Models are built as layered systems with alternating steel and rubber layers. Rubber and steel layers have nonlinear and linear performance, respectively [24]. They are connected together via vulcanization process. Steel end plates are used on the top of first rubber and in the bottom of the end rubber. Full 3D models are used to illustrate the geometry and loading conditions of each EBs. Full integration solid hybrid element (C3D8H) and full integration solid element (C3D8) is employed to model the rubber and steel layers, respectively. Fixed boundary condition is considered at the bottom and boundary condition at the top is similar to the bottom but only allows to move freely in lateral and vertical directions. Various material behavior such as hyper-elastic and viscoelastic can be used to define properties of rubber-like materials in ABAQUS. The hyper-elastic behavior is described with strain energy potential function. Several forms of stain energy potentials are existing in ABAQUS. Three types of hyper-elastic models are more common: Neo-Hookean [42] Rivlin [43] and Ogden [44]. The Neo-Hookean material model is the simplest method for modeling the hyper-elastic materials and works based on initial shear modulus and incompressibility. Kim et al. [45] comprehensively compared Neo-Hookean, Rivlin, and Ogden models in describing rubber materials. The Rivlin model is usually used for structural components with local strain values up to $\sim$ 200%, while the Ogden hyper-elastic model is successful in numerical analysis for cases with strain values as high as 700%

[45]. The exponents of the stretch ratio are real numbers for the Ogden model and integers for the Rivlin model. Accordingly, the Ogden model offers better performance and flexibility than the Neo-Hookean and Rivlin model [45]. Thus, the Ogden hyper-elastic model is selected in this study. Consideration of a strain energy density function is important in seismic bearings because the high pressures involved in their loading can lead to volumetric strain in the rubber as high as 10% [44]. The strain energy density function is defined in Eq. (1):

$$U=\sum_{i=1}^{2}\frac{2\mu_i}{\alpha_i^2}\left(\bar{\lambda}_1^{\alpha_i}+\bar{\lambda}_2^{\alpha_i}+\bar{\lambda}_3^{\alpha_i}-3\right)+4.5K\sum_{i=1}^{N}\left(J^{\beta}-1\right)^2 \quad (1)$$

where $\bar{\lambda}_1$, $\bar{\lambda}_2$ and $\bar{\lambda}_3$ are the principal values of right stretching tensor and J is the elastic volume ratio. α_i and μ_i denote the empirically-determined material constants.

2. Validation analysis

The numerical model is validated by comparing the results with the experimental findings of Yamamoto et al. [40] and Minewaki et al. [41]. They reported experimental results for an elastomeric rubber bearing with geometric properties that showed in Table 1. The cyclic horizontal force-displacement behavior predicted by the finite element model is compared with those reported by Yamamoto et al. [40] and Minewaki et al. [41]. Fig.1 shows validation model, loading and boundary condition.

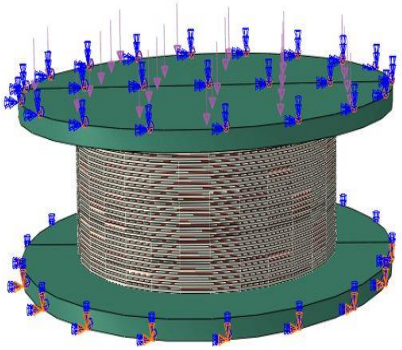

Fig.1 validation model

Table1 properties of validation model

Geometric properties	
Thickness of rubber layer	4.7 mm
Number of rubber layer	30
Total thickness of rubber layer	141 mm
Thickness of steel plate	3.1 mm
Number of steel plate	29
Thickness of steel end plate	25 mm
Diameter of rubber and steel layer	700 mm
Diameter of inner hole	15mm
Diameter of anchor steel plates	1000 mm

3.1 Material properties

In this research material properties for rubber and steel extracted from experimental work [40]. Ogden function used for rubber simulation and parameters are $\alpha_1 = 1.6$, $\alpha_2 = 6.2$, $\mu_1 = 0.41$ MPa, $\mu_2 = 0.0012$ MPa, and $\beta = 1/3$ [45]. These parameters can be obtained from the experimentally-measured stress-strain curves under different pressure levels. The bulk modulus was K = 1000 MPa [45]. Initial shear modulus (G) and Poisson's ratio (ν) can be obtained from Eq. (2) and Eq. (3), respectively [45]:

$$G=\alpha_1\mu_1+\alpha_2\mu_2=0.66344\,\text{MPa} \quad (2)$$

$$\nu=\frac{3K}{G}-\frac{2}{\left(\frac{6K}{G}\right)}-2=0.49989 \quad (3)$$

The steel shim layers do not enter to the nonlinear region during analysis and elasticity modulus is E=205 GPA, Poisson's ratio is $\nu = 0.3$ and yield stress is σ_y= 235 MPa [45].

International Journal of Advanced Structural Engineering (2022) 12 : 15319–630
https://doi.org/10.1007/s40091-019-00252-8

3.2 Hysteresis behavior

Hysteresis parameters (stress scaling factor, S, creep parameter, A, effective stress exponent, m, and creep strain exponent, C) were taken from Bergström and Boyce [46]. Given that in this study the cyclic behavior of the isolator is evaluated, the inclusion of hysteresis parameters is essential. In other words, in the finite element analysis, the hysteresis loop is formed upon the introduction of these parameters for the rubber material. The stress scaling factor defines the ratio of the stress tolerated under instantaneous loading and affects the isolator damping ratio. The creep parameter refers to the expression for the effective creep strain rate. This constant also maintains the dimensional consistency in the equation. The effective stress exponent is generally greater than 1, characterizing the effective stress dependence of the effective creep strain rate. These parameters are listed in Table 2. It should be noted that these parameters are dimensionless. In the work of Kalfas et al. [20], stress scaling factor, creep parameter, effective stress exponent, and creep strain exponent were taken as S=1.6, A = 0.56, m = 4, and C = -1, respectively. Rahnavard and Thomas [24] considered the following parameters: stress scaling factor, S=1.6, creep parameter, A = 0.56, effective stress exponent, m = 4, and creep strain exponent, C =0. In this regard, various values of S, A, m, and C were considered for validation and the closest values to the experimental result will be considered. For loading procedure, uniform vertical load (14 MPa) was applied then laterally displaced with a cyclic pattern (displacement was applied at the top of the isolator). Shear force-displacement is shown in Fig.2.

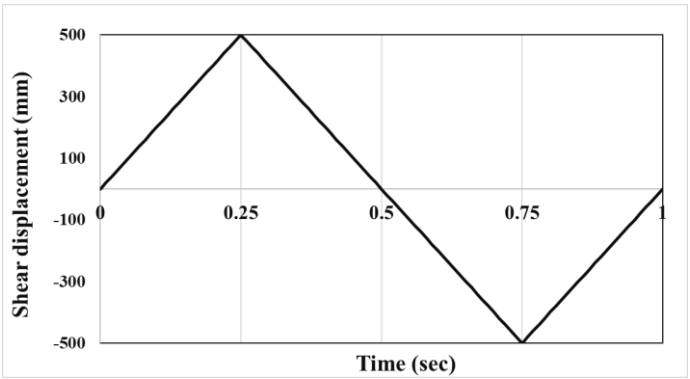

Fig.2 Cyclic loading

Table 2 Hysteresis parameters

Various types	Stress scaling factor (S)	Creep parameter (A)	Effective stress exponent (m)	Creep strain exponent (C)
Type 1	1.6	0.56	4	0
Type 2	1.6	0.56	4	-1
Type 3	1.6	1.67	2	-1
Type 4	1.6	2.89	1	-1
Type 5	2.0	1.67	2	-1
Type 6	2.0	2.89	1	-1
Type 7	1.1	1.67	2	-1

As shown in Fig.3-a to Fig.3-e, various hysteresis parameters were adopted and isolator force-displacement response was compared with experimental work.

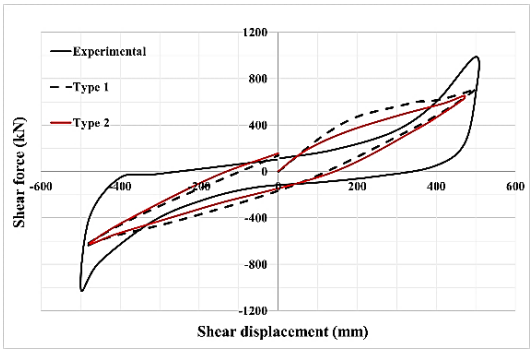

Fig.3-a

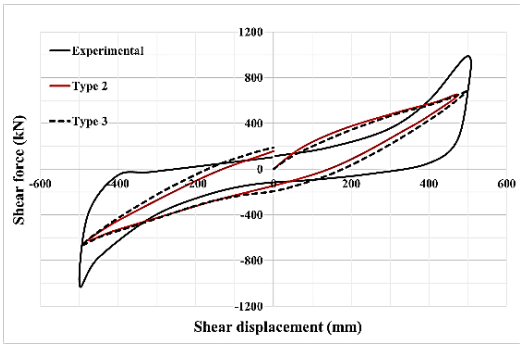

Fig.3-b

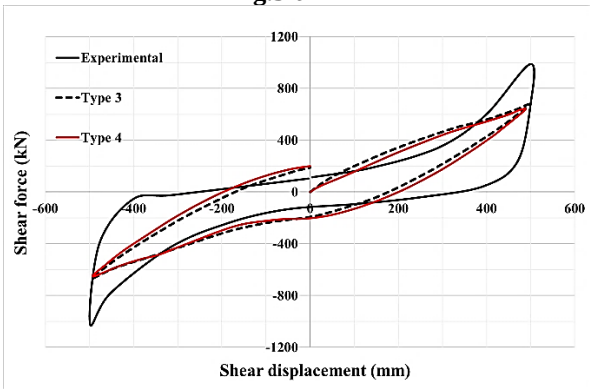

Fig.3-c

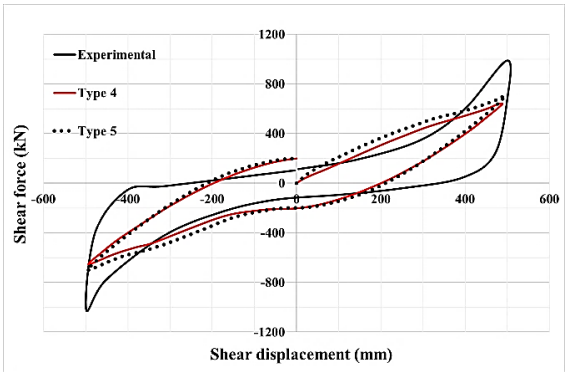

Fig.3-d

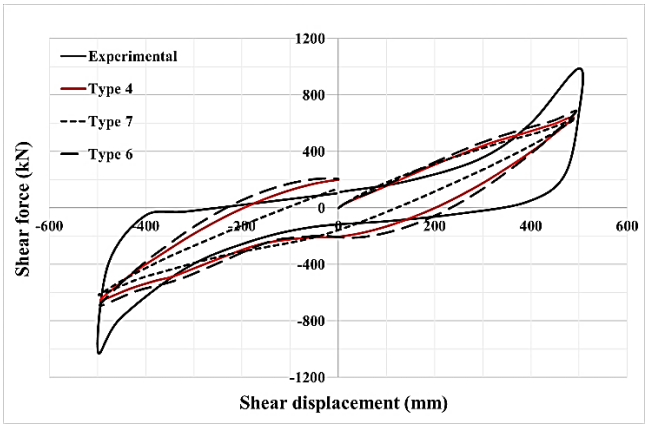

Fig.3-e

Fig3 Comparison between experimental and numerical results with various hysteresis parameters

As indicated in Fig3, hysteresis parameters related to Type 4 in Table 2 led to closest result to experimental work.

Except the hysteresis validation analysis simple shear displacement analysis is done and compared with experiment result. In this analysis vertical load (14MPa) is applied on isolator then laterally displaced. This analysis with various mesh size is performed. Mesh properties and elements number was defined in Table 3.

Table 3 Mesh properties

Mesh ID	Seed size (mm)	No. of rubber elements	No. of steel elements	No. of anchor elements	Total elements	Result
Mesh 1	200	24	12	16	1100	Not converge
Mesh 2	150	32	16	36	1496	Completed
Mesh 3	100	72	36	90	3384	Completed
Mesh 4	90	112	56	100	5184	Completed
Mesh 5	70	180	90	168	8520	Completed
Mesh 6	60	264	132	240	12228	Not converge
Mesh 7	60	264	132	100	11948	Not converge
Mesh 8	60	264	132	340	12428	Completed
Mesh 9	40	540	270	896	25822	Not converge

Fig.4 shows the validation results and indicated that acceptable accuracy is exist between experimental and finite element analysis.

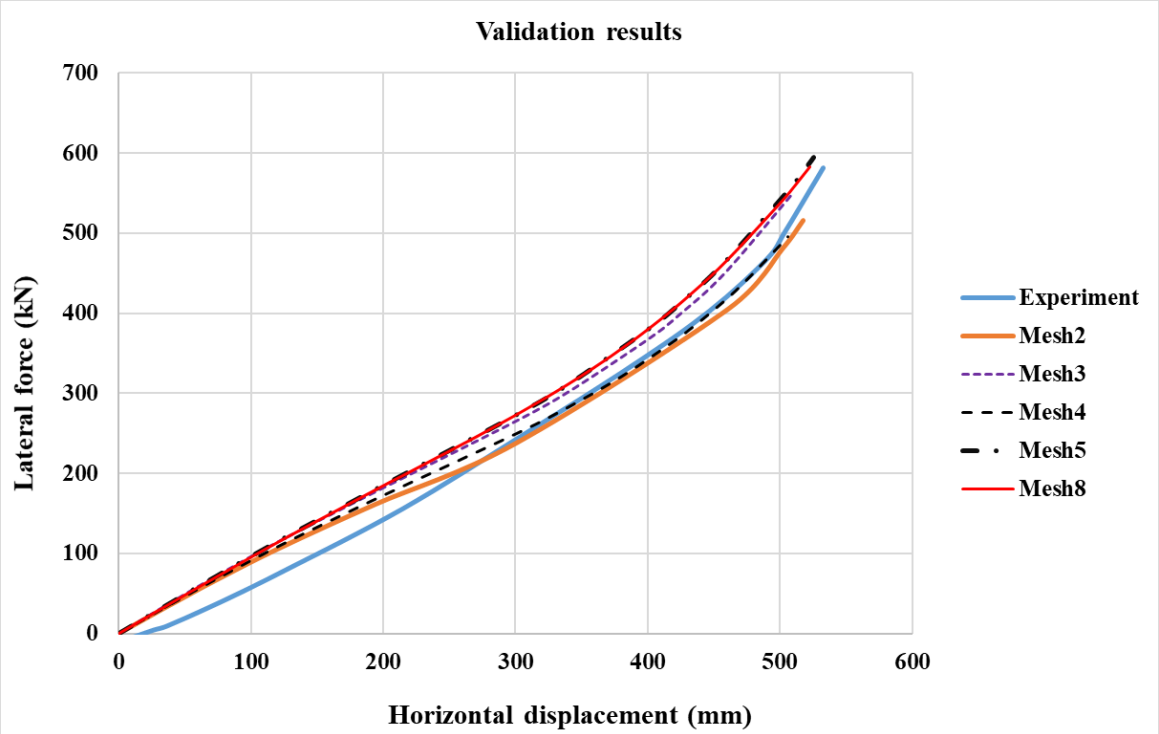

Fig.4 Validation results of simple shear analysis

4. Case study

Full-scale elastomeric bearings are defined with the previously-described rubber and steel material properties (section 3.1). The validated hysteresis parameters (Type 4) and hyper-elastic behavior (Ogden function) are used to describe the rubber behavior. Ogden parameters are defined in Section 3 as presented in Table 4.

Table 4 Rubber and steel material properties

Rubber (Ogden parameters)				Steel (elastic)	
μ_1 (MPa)	μ_2 (MPa)	α_1	α_2	E (MPa)	Poison ratio
0.41	0.0012	1.6	6.2	200 000	0.3

The elastomeric bearing is circular with the following geometrical features; diameter of circular rubber and steel layers: 500 mm, the diameter of the inner hole:10 mm, the diameter of steel end plates (anchor plates): 700 mm and thickness of steel end plate: 25

mm. Various shape factors (S) is considered. As an important parameter with a key role in the shear behavior of elastomeric bearings, shape factor can be defined as the ratio of the loaded area to free loaded area of rubber pad (Eq. (4)). Mordini and Strauss [47] investigated the cyclic behavior of elastomeric bearing and introduced Eq. (5) and Eq. (6) for calculating the horizontal stiffness and damping, respectively.

$$S = \frac{D_o - D_i}{4t_r} \quad (4)$$

D_o: outer diameter D_i: inner diameter (inner hole) t_r: thickness of one rubber layer

$$K_h = \frac{F_{max} - F_{min}}{\Delta_{max} - \Delta_{min}} \quad (5)$$

$$\xi = \frac{2W_s}{\pi K_h \left(\Delta_{max} - \Delta_{min}\right)^2} \quad (6)$$

In Eq. (5) and Eq. (6), F_{max} and F_{min} are maximum and minimum forces in every cycle in hysteresis behavior, respectively. W_s shows the area of each hysteresis cycle, K_h denotes the horizontal stiffness and Δ_{max} and Δ_{min} represent the maximum and minimum lateral displacements, respectively. Fig.5 shows force-displacement behavior of elastomeric rubber bearing (isolator).

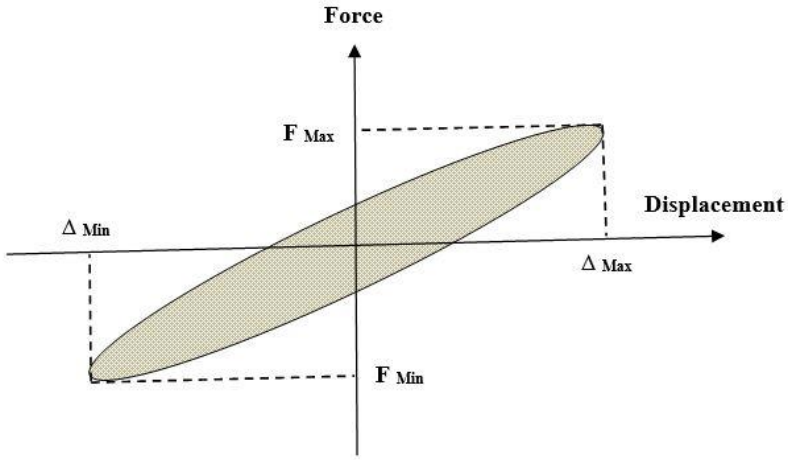

Fig.5 Force-displacement behavior of EB

Various models of elastomeric bearing through using different shape factors are introduced in Table 5. The total height of elastomeric bearings in all models is constant. Fig.6 shows the various models.

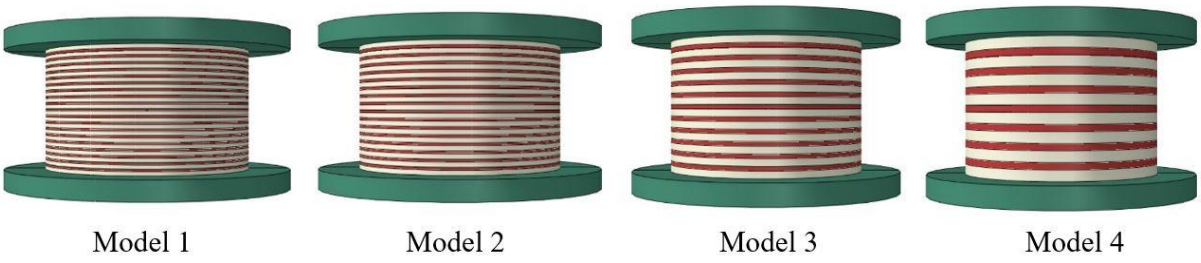

Fig.6 EBs with various shape factors

Table 5 various models of elastomeric bearing and shape factor

Model ID	Thickness of rubber layers (mm)	Number of rubber layers	Thickness of steel layers (mm)	Number of steel layers	Shape factor
Model 1	5	20	3	19	24.5
Model 2	5.89	17	3.563	16	20.8
Model 3	8.333	12	5.182	11	14.7
Model 4	12.5	8	8.143	7	9.8

The cycling loading pattern is depicted in Fig.7.

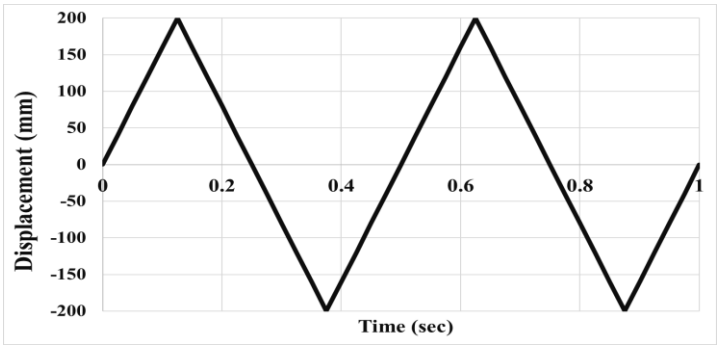

Fig.7 loading pattern

4.1 Numerical analysis

As the shape factor is a key parameter in elastomeric bearing design, four various shape factors have been defined in Table 5. These four models will be under various vertical pressures (10, 6, 2, and 0MPa) and then hysteresis loadings will be applied as shown in Fig.7. Figs.8 to 11 are indicating the hysteresis behavior of models under various vertical pressures.

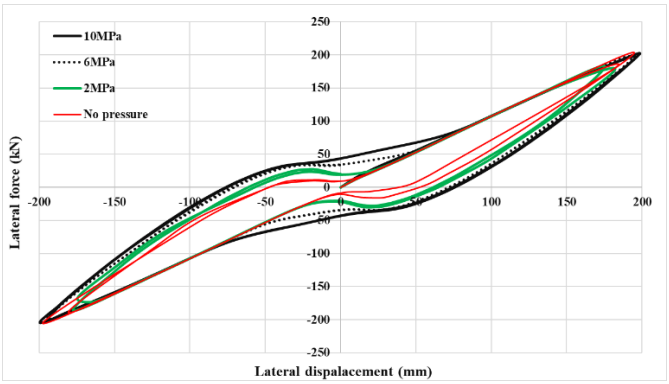

Fig.8 Hysteresis behavior of Model 1

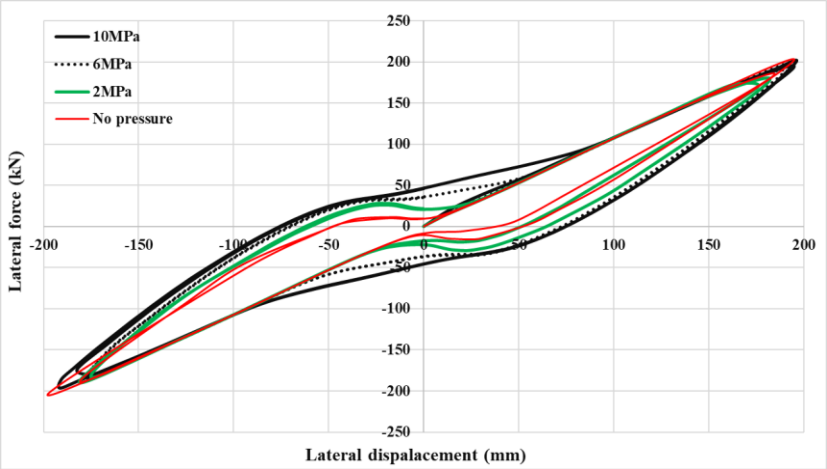

Fig.9 Hysteresis behavior of Model 2

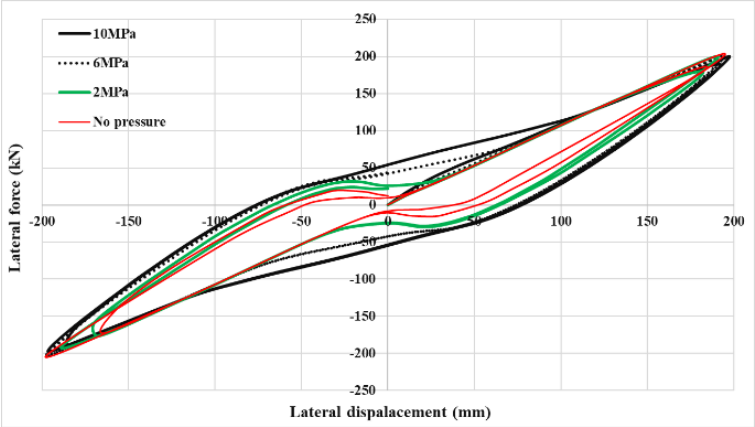

Fig.10 Hysteresis behavior of Model 3

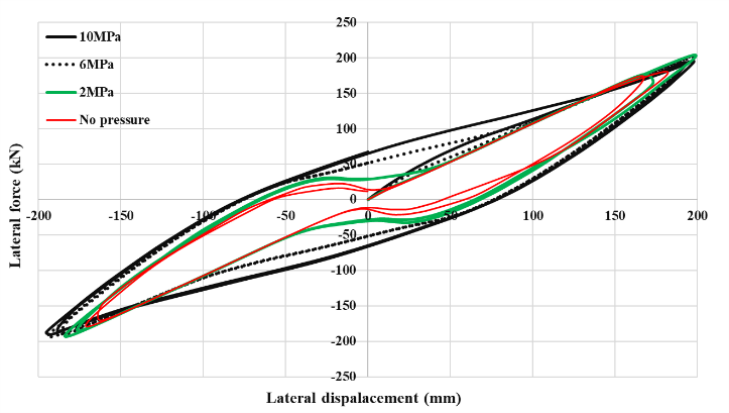

Fig.11 Hysteresis behavior of Model 4

4.2 Results

Hysteresis damping is calculated for models 1 to 4 in cycle #1 and cycle #2 of loading and effect of various shape factor and vertical pressure on hysteresis damping are evaluated. Fig.12 shows the effect of shape factor and vertical pressure on hysteresis damping. An increase in vertical pressure led to enhance the hysteresis damping of elastomeric bearings with various shape factors. Table 5 shows the variation percentage of damping in cycle #2 compared to cycle #1. Table 6 also lists the amount of damping increment for different shape factors and vertical pressures compared with model 4 which had no vertical pressure.

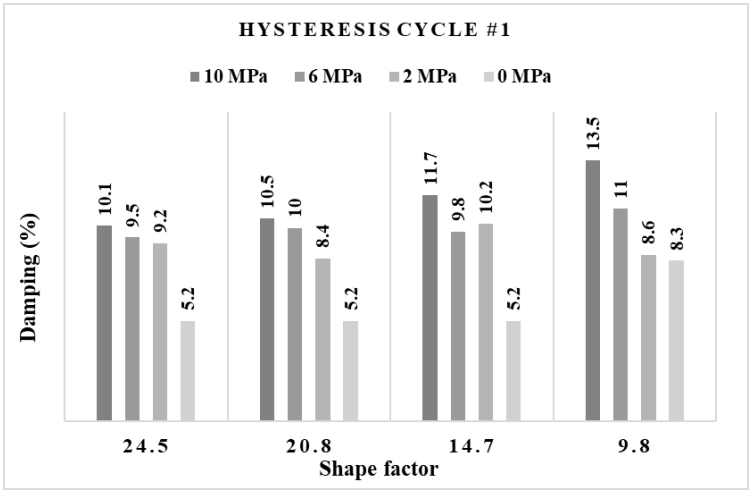

Fig.12-a cycle #1

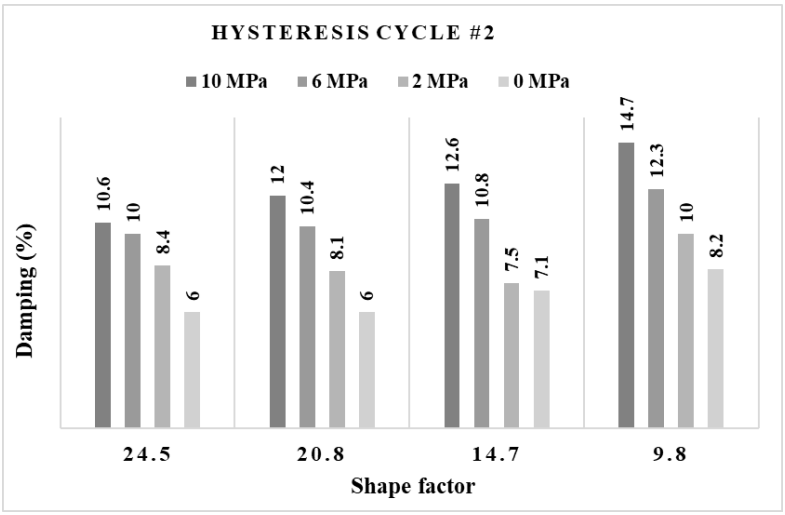

Fig.12-b cycle #2

Fig.12 Hysteresis damping in various shape factor and vertical load

Table 6 Relative change in damping of cycle #2 to cycle #1 (%)

Vertical pressure (MPa)	S=24.5	S=20.8	S=14.7	S=9.8
10	5	14.3	7.7	8.9
6	5.3	4	10.2	11.8
2	-8.7	-3.6	-26.5	16.3
0	15.4	15.4	36.5	-1.2

(+: Increase and -: Decrease)

Table 7 Effect of vertical load on damping

Vertical pressure	cycle #1				cycle #2			
	S=24.5	S=20.8	S=14.7	S=9.8	S=24.5	S=20.8	S=14.7	S=9.8
	Relative change in damping under specified vertical load to without vertical load of EBs (%)							
10 MPa	94.2	101.9	125	62.7	76.7	100	77.5	79.3
6 MPa	82.7	92.3	88.5	32.5	66.7	73.3	52.1	50
2 MPa	76.9	61.5	96.2	3.6	40	35	5.6	22

Table 8 indicates the effect of shape factor on hysteresis damping. As can be seen, higher hysteresis damping was observed in lower shape factors. For example, in cycle #2, under 10 MPa vertical load, hysteresis damping was increased by 38.7% for S=9.8 as compared to S=24.5. This increase in hysteresis damping was 22.5% for the case with S=9.8 as compared with shape factor of 20.8. The hysteresis damping increase of the model with S=9.8 was 16.7% compared to the one with S=14.7. Under 6 MPa vertical pressure, however, the hysteresis damping increased by 23% for the model with S=9.8 relative to the model having S=24.5 and incremented by 18.3% in the model with S=9.8 to the one with S=20.8 and increased by 13.9% in the model via S=9.8 to the model with S=14.7. Under 2 MPa vertical load, hysteresis damping raised by 19% in the model with S=9.8 compared with S=24.5 and increased by 23.5% in the model with S=9.8 to the model with S=20.8 and increased by 13.4% in the model with S=9.8 to the model with S=14.7. In 0 MPa vertical load (no pressure), hysteresis damping increased by 36.7% in the model with S=9.8 relative to the model with S=24.5 and increased by 36.7% in the model via S=9.8 to the one having S=20.8 and increased by 15.5% in the model via S=9.8 relative to the one with S=14.7.

Table 8 Percentage of damping variation for various shape factor ratio

Vertical pressure (MPa)	Damping variation of model 4 to model 1		Damping variation of model 4 to model 2		Damping variation of model 4 to model 3	
	Cycle #1	Cycle #2	Cycle #1	Cycle #2	Cycle #1	Cycle #2
10	33.7	38.7	28.6	22.5	15.4	16.7
6	15.8	23	10	18.3	12.3	13.9
2	-6.5	19	2.4	23.5	-15.7	13.4
0	59.6	36.7	59.6	36.7	59.6	15.5

5. Conclusion

In this research, two main goals were pursued. The first goal was to determine the appropriate parameters for modeling the cyclic behavior of isolators in finite element analysis, and the second goal was to investigate the effect of shape factor and vertical load on the hysteresis damping of isolators. The results obtained are summarized as follows:

- The hysteresis parameters such as stress scaling factor =1.6, creep parameter=2.89, effective stress exponent= 1, and creep strain exponent=-1 led to closest results in comparison with experimental work.
- Decrease in the shape factor led to increase in damping.
- Damping increases with the increase in the vertical pressure.

References

Haringx, J. A., (1948). On highly compressible helical springs and rubber rods and their application for vibration-free mountings I. Philips Res.

Kelly, J. M., (1997). Earthquake-Resistant Design with Rubber. Switzerland, Springer.

Buckle, I. G., Liu, H., (1993). Stability of elastomeric seismic isolation systems, Proc., Seminar on Seismic Isolation, Passive Energy Dissipation and Control, Applied Technology Council, Redwood City, CA, 293–305.

Buckle, I. G., Liu, H., (1994). Critical loads of elastomeric isolators at high shear strain, Proc., 3rd U.S.-Japan Workshop on Earthquake Protective Systems for Bridges, National Center for Earthquake Engineering Research, Buffalo, NY.

Aiken, I. D., Kelly, J. M., Tajirian, F. F., (1989). Mechanics of low shape factor elastomeric seismic isolation bearings, Earthquake Engineering Research Center, Univ. of California, Berkeley, CA, UCB/EERC-89/ 13.

Civil Engineering Research Foundation (CERF), Evaluation findings for Scougal Rubber Corporation high damping rubber bearings, Rep. No. HITEC 98-11 40373, Washington, DC, 1998a.

Civil Engineering Research Foundation (CERF), Evaluation findings for Skellerup base isolation elastomeric bearings, Rep. No. HITEC 98-11 40376, Washington, DC, 1998b.

Civil Engineering Research Foundation (CERF), Evaluation findings for Tekton, Inc., steel rubber bearings, Rep. No. HITEC 98-10 40365, Washington, DC, 1998c.

Civil Engineering Research Foundation (CERF), Summary of evaluation findings for the testing of seismic isolation and energy dissipating devices, Rep. No. 40404, Washington, DC, 1999.

Buckle, I., Nagarajaiah, S., Ferrell, K., (2002). Stability of elastomeric isolation bearings: Experimental study, J. Struct. Eng., 128:1, 3–11.

Warn, G. P., Whittaker, A., Constantinou, M., (2007). Vertical stiffness of elastomeric and lead–rubber seismic isolation bearings, J. Struct. Eng., 133.9, 1227– 1236.

Sanchez, J., Masroor, A., Mosqueda, G., Ryan, K., (2012). Static and dynamic stability of elastomeric bearings for seismic protection of structures, J. Struct. Eng., 139.7, 1149–1159.

Han, X., Kelleher, C. A., Warn, G. P., Wagener, T., (2013). Identification of the controlling mechanism for predicting critical loads in elastomeric bearings, J. Struct. Eng., 139.12: 04013016.

Nagarajaiah, S., Ferrell, K., (1999). Stability of elastomeric seismic isolation bearings, Journal of Structural Engineering, 125.9, 946-954.

Warn, G. P., Whittaker, (2006). Property modification factors for seismically isolated bridges, J. Bridge Eng., 11.3, 371–377.

Warn, G. P., Whittaker, Constantinou, M., (2007) Vertical stiffness of elastomeric and lead–rubber seismic isolation bearings, J. Struct. Eng., 133.9, 1227-1236.

Warn, G., Weisman J., (2011). Parametric finite element investigation of the critical load capacity of elastomeric strip bearings, Eng. Struct., 33.12, 3509–3515.

Weisman, J., Warn G., (2011). Stability of elastomeric and lead rubber seismic isolation bearings, J. Struct. Eng., 138.2, 215–223.

Kumar, M., Whittaker, A. S, Constantinou, M. C., (2014). An advanced numerical model of elastomeric seismic isolation bearings, Earthquake Engineering and Structural Dynamics, 43.13, 1955-1974.

Kalfas, K. N., Mitoulis, S. A., Katakalos, K., (2017a). Numerical study on the response of steel-laminated elastomeric bearings subjected to variable axial loads and development of local tensile stresses, Engineering Structures, 134, 346-357.

Kalfas, K. N., Mitoulis, S. A., Katakalos, K., (2017b). Numerical study on bridge elastomeric bearings subjected to large shear strain with emphasis on local tension, 16th World Conference on Earthquake Engineering, 9-13 January, Santiago, Chile.

Kalfas, K. N., Mitoulis, S. A., Konstantinidis, D., (2020). Influence of the steel reinforcement on the vulnerability of elastomeric bearings, Journal of Structural Engineering, DOI: 10.1061/(ASCE)ST.1943-541X.0002710.

Kalfas, K. N., Mitoulis, S. A., (2017c). Performance of steel-laminated rubber bearings subjected to combinations of axial loads and shear strains, Procedia Engineering, 99, 2979-2984.

Rahnavard, R., Thomas, R. J., (2019). Numerical evaluation of steel-rubber

isolator with single and multiple rubber cores, Engineering Structures, 198, 109532.

Forcellini, D., Mitoulis, S. A., Kalfas, K. N., (2017). Study of the response of elastomeric bearings with 3D numerical simulations and experimental validation, Computational Methods in Structural Dynamics and Earthquake Engineering (COMPDYN) Conference, Rhodes Island, Greece, 15-17 June.

Forcellini, D., (2016). 3D Numerical simulations of elastomeric bearings for bridges, Innovative Infrastructure Solution, 1.1.

Kalfas, K. N., Forcellini, D., (2020). A developed analytical non-linear model of elastomeric bearings verified with numerical findings, International Conference on Structural Dynamics (EURODYN), Athens, Greece, 22-24 June.

Forcellini, D., Kelly, J. M., (2014). Analysis of the large deformation stability of elastomeric bearings, Journal of Engineering Mechanics, 140.6:04014036.

Kelly, J. M., Takhirov, S. M., (2000). Tension buckling in multilayer elastomeric isolation bearings, Journal of Mechanics of Materials and Structures, 2, 1591–1605.

Naeim, F. and Kelly, J. M., (1999). Design of seismic isolated structures: from theory to practice). John Wiley & Sons.

Warn, G. P., Whittaker, A. S., (2006). A study of the coupled horizontal-vertical behavior of elastomeric and lead-rubber seismic isolation bearings. Tech. Rep. MCEER-06-001, University at Buffalo, State University of NewYork.

Tsai, H., C. and Hsueh, S., J., (2001). Mechanical properties of isolation bearings identified by a viscoelastic model. International Journal of Solids and Structures, Volume 38, Issue 1, 5 January 2001, Pages 53-74. https://doi.org/10.1016/S0020-7683(00)00010-X.

Karbakhsh Ravari, A. and Bin Othman, I. and Binti Ibrahim, Z. and Ab-Malek, K. (2011). P-Δ and end rotation effects on the influence of mechanical properties of elastomeric isolation bearings. Journal of Structural Engineering, American Society of Civil Engineering.

Forcellini, D., (2018b). Seismic assessment of a benchmark based isolated ordinary building with soil structure interaction, Bulletin of Earthquake Engineering, 16.5, 2021-2042.

Canini, A., Forcellini, D, (2017). 3D numerical simulations of a base-isolated residential building with soil structure interaction", Computational Methods in Structural Dynamics and Earthquake Engineering (COMPDYN) Conference, Rhodes Island, Greece, 15-17 June.

Gauron, O., Saidou. A., Busson,A., Siqueira, G. H., (2018). Experimental determination of the lateral stability and shear failure limit states of bridge rubber bearings. Journal of Engineering Structures 174. P.39-48, Elsevier, https://doi.org/10.1016/j.engstruct.2018.07.039.

Forcellini, D., (2018a). Cost Assessment of isolation technique applied to a benchmark bridge with soil structure interaction, Bulletin of Earthquake Engineering, 15.1, 51-69.

Kazeminezhad, E., Kazemi, M. T., Mirhosseini, M. (2019). Assessment of the vertical stiffness of elastomeric bearing due to displacement and rotation. International Journal of Non-Linear Mechanics, Elsevier. DOI: https://doi.org/10.1016/j.ijnonlinmec.2019.103306.

Hibbett, Karlsson, Sorensen, 1988. ABAQUS/standard: User's Manual, vol. 1. Hibbitt, Karlsson & Sorensen.

Yamamoto, M., Minewaki, S., et al., (2009). Full-scale tests and analytical modeling of high-damping rubber bearings under two horizontal directional loading, J. of Struct. and Constr. Eng., No. 638, 639-645, AIJ, 2009, Japan.

Minewaki, S., Yamamoto, M., et al., (2009). Performance Tests of Full-Size Isolators for Super Highrise Isolated Buildings. J. of Struct. Eng., Vol. 55B, 469-477, AIJ, 2009, Japan.

Boulanger, P., Hayes, M., (2001). Finite amplitude waves in Mooney-Rivlin and hadamard materials. Topics in Finite Elasticity. International Center for Mechanical Sciences.

Rivlin, R. S. Large elastic deformations of isotropic materials IV. Further developments of the general theory. Philos

Trans Roy Soc Lond Ser A: Math Phys Eng Sci 1948;241(835):379–97. The Royal Society.

Ogden, W. R., Large deformation isotropic elasticity–on the correlation of theory and experiment for incompressible rubberlike solids. Proc Roy Soc Lond A 1972;326(1567):565–84. The Royal Society.

Beomkeun, K., Beom, L. S., Jayone, L., Sehyun, C., Hyungmin, P., Sanghoon, Y., (2012). A comparison among Neo-Hookean Model Mooney-Rivlin Model, and Ogden model for chloroprene rubber. Int J Precis Eng Manuf 2012;13(5):759–64.

Bergström, J. S., Boyce, M. C., Constitutive modeling of the large strain time dependent behavior of elastomers. J Mech Phys Solids 1998;46:931–54.

Mordini, A., Strauss A., (2008). An innovative earthquake isolation system using fiber reinforced rubber bearings. Engineering Structures 2008; 30 (10): 2739–2751.

Bhuiyan, A. R., Okui, Y., Mitamura, H., Imai, T., (2009). A rheology model of high damping rubber bearings for seismic analysis: Identification of nonlinear viscosity. International Journal of Solids and Structures, Volume 46, Issues 7–8, April 2009, Pages 1778-1792. https://doi.org/10.1016/j.ijsolstr.2009.01.005.